JOURNAL OF AIRCRAFT
Vol. 32, No. 4, July–August 1995

Aeroelastic Analysis of a Flexible Control Surface with Structural Nonlinearity

In Lee* and Seung-Ho Kim†
Korea Advanced Institute of Science and Technology, Taejon 305-701, Republic of Korea

This article is concerned with a time domain approach to the flutter analysis of a flight vehicle control surface with concentrated nonlinearities. In this study, an elastic model of a control surface with root freeplay nonlinearity in pitch is considered. A finite element structural model is used for structural analysis and a doublet lattice unsteady aerodynamic model is used for the calculation of aerodynamic loads. In approximating the frequency domain aerodynamic forces, the least-square rational function approximating method is used with an optimizing algorithm. To transform the frequency domain aerodynamic forces to the time domain forces, the method of Brace and Eversman is used. To reduce the problem size and the computation time, the fictitious mass modal approach is used, which can afford the possible local change of structural properties. The effects of the initial conditions and the magnitude of nonlinearity on the aeroelastic characteristics are examined. The aeroelastic responses are sensitive to initial conditions. Limit cycle oscillation and chaotic motion are observed in this study. The presence of freeplay makes the divergent flutter speeds larger than those of a linear case.

Nomenclature

$[A_i]$ = aerodynamic approximation coefficient matrix
b = half-chord length
$[C]$ = structural damping matrix
E = Young's modulus
$\{F\}$ = external force vector
$f(\alpha)$ = nonlinear elastic restoring force
$[GK]$ = generalized stiffness matrix
$[GM]$ = generalized mass matrix
$[K]$ = stiffness matrix
K_α = pitch spring stiffness
k = reduced frequency, $\omega b/U_\infty$
k_m = constant for aerodynamic approximation
$[M]$ = mass matrix
$[M_f]$ = fictitious mass matrix
$[Q]$ = aerodynamic influence coefficient matrix
q = dynamic pressure
$\{R(u)\}$ = elastic restoring force
s = freeplay angle
U_∞ = freestream velocity
$\{u\}$ = nodal displacement vector
$\underline{z}_m$ = augmented states
α = pitch rotation angle
$\delta(t)$ = Dirac delta function
ρ = density of air
$[\phi_b]$ = mode vector of basic system
$[\phi_f]$ = mode vector of fictitious mass model
$[\chi_b]$ = transformation matrix of basic system
ω = natural frequency in radian
ω_f = natural frequency of fictitious mass model in radian
$\dot{(\ )}$ = $\mathrm{d}(\ )/\mathrm{d}t$
$\ddot{(\ )}$ = $\mathrm{d}^2(\ )/\mathrm{d}t$
$\underline{(\ )}$ = generalized coordinate
$\bar{(\ )}$ = amplitude of harmonic motion

Subscripts
b = basic system
f = fictitious mass model
0 = initial condition

Received Aug. 18, 1993; revision received Dec. 20, 1994; accepted for publication Feb. 17, 1995.

*Associate Professor, Department of Aerospace Engineering, 373-1 Kusong-Dong, Yusong-Gu. Member AIAA.
†Graduate Research Assistant, Department of Aerospace Engineering.

Introduction

MOST aeroelastic analyses of an aircraft have been performed under the assumption of aerodynamic and structural linearity. The progress of the aeroelastic analysis techniques and the computational capability enables us to analyze the nonlinear characteristics. The nonlinearities in aeroelastic analysis are divided into aerodynamic and structural properties. The causes of aerodynamic nonlinearity are shock wave, viscosity, aerodynamic heating, turbulence, etc. Structural nonlinearities are subdivided into distributed nonlinearities and concentrated ones. Distributed nonlinearities are spread over the entire structure like material nonlinearity, but concentrated nonlinearities act locally as in a control mechanism or an attachment of external stores. Examples of concentrated nonlinearities are freeplay, friction, hysteresis, and preload. Concentrated structural nonlinearities are generated from a worn or loose hinge of the control surface, joint slippage, and manufacturing tolerance. Since these nonlinearities are the function of the amplitude and the path of the motion, the flutter speed and response characteristics are different from the linear case. The response of the nonlinear aeroelastic system typically has four types of responses, i.e., 1) the flutter, 2) divergence, 3) limit cycle oscillation, and 4) chaotic motion. The flutter and divergence are unbounded unstable motions with increasing amplitude, whereas the limit cycle oscillation and the chaotic motion are bounded motion. The limit cycle is a periodic oscillation consisting of a limited number of frequencies and amplitudes. The chaotic motion is a nonperiodic oscillation consisting of a multitude of frequencies and amplitudes. Since the limit cycle oscillation and the chaotic motion occur below the divergent flutter speed, it is important to know the characteristics of the nonlinear aeroelastic response in designing a flight vehicle.

The analysis methods of a nonlinear aeroelastic problem are divided into a frequency domain approach and a time domain approach. In a frequency domain approach, the describing function method[1] and asymptotic expansion method[2] are available. These methods are convenient for the examination of the system characteristics. However, these methods cannot give the detailed motion characteristics because of the assumption of

harmonic motion. A time domain method integrating the equations of motion can give the detailed motion characteristics. Although a time domain approach is inconvenient for the investigation of the whole system characteristics, it is the only possible method to examine the chaotic response. The present study utilizes the time domain approach.

Time domain approaches to the nonlinear aeroelasticity were performed in the 1950s using an analog computer by Woolston et al.[3] to understand the nonlinear phenomena. They analyzed the simple system including freeplay, hysteresis, and cubic nonlinearity. They dealt with a two-dimensional model and Wagner's indicial response function. They showed that the limit cycle oscillation may occur below the linear flutter boundary. McIntosh et al.[4] made experimental work with the wind-tunnel model of 2 degrees of freedom (DOF). Lee[5] developed an iterative scheme for multiple nonlinearities using the describing function method and the structural dynamics modification technique. Yang and Zhao[6] studied the limit cycle oscillation of an airfoil with pitch nonlinearity subject to incompressible flow using the Theodorsen function that is correct for harmonic motion. They made a comprehensive study of limit cycle flutter. Zhao and Yang[7] also studied the chaotic responses of an airfoil with cubic nonlinearity in pitch subject to steady incompressible flow. Brase and Eversman[8] developed the method of converting harmonic aerodynamic force to a transient one using a linear superposition principle. They analyzed the flutter characteristics of a 2-DOF airfoil model and an 8-DOF F-18 stabilizer with freeplay nonlinearities. For a normal mode approach, they used a flexible mode inertially coupled with a rigid body mode. They found that the divergent flutter speed of the nonlinear system with freeplay is higher than that of the linear case, depending on the initial conditions and the magnitude of freeplay, and found a jump response in a two-dimensional model with a pitch freeplay model. Hauenstein et al.[9,10] performed an analytical and experimental study on the chaotic response of aerosurface with pitch and plunge freeplay structural nonlinearities. They used a beam-rod finite element structural model, two-dimensional aerodynamics, and a mode synthesis method. They showed qualitatively good results between analytical and experimental results. They concluded from the results that the chaotic motions do not occur with the presence of a single nonlinearity, but Price et al.[11,12] pointed out that this is not true. They made a comprehensive aeroelastic study of two-dimensional airfoil with pitch nonlinearities like freeplay, cubic, and bilinear stiffness.

Previous studies have mainly dealt with a simple or rigid aerosurface. There are not enough studies for the flexible aerosurface with nonlinearities and the general analysis method was not properly established for such a nonlinear system. The purpose of the present study is to analyze the aeroelastic characteristics of the flexible control wing of a flight vehicle with root freeplay nonlinearity. In this study, an elastic model of the control surface with freeplay nonlinearity is examined. Finite element plate model and doublet lattice unsteady aerodynamic model[13] are combined for the calculation of the aeroelastic response. In approximating the frequency domain aerodynamic forces, Roger and Abel's least-square rational function approximating method[14] is used with optimizing algorithm. To transform the frequency domain aerodynamic forces to the time domain, the method of Brace and Eversman is used. To reduce the problem size and the computation time, Karpel's fictitious mass (FM) modal approach[15,16] is used, which can afford the possible local change of stuffiness. The effects of the initial conditions and the magnitude of nonlinearity on the aeroelastic characteristics are investigated.

Nonlinear Aeroelastic Analysis

FM Modal Approach

Generally, aeroelastic analysis is conducted in the generalized modal coordinate to reduce the computation time and memory requirement. In nonlinear aeroelastic problems, structural properties are varying as the displacement changes. Hence, using a constant normal mode from a fixed structural model gives inaccurate results. To overcome this problem, Karpel proposed the FM method.[15,16] In this method, a large FM is added to the DOF of mass matrix where structural change will occur. Then, the normal modes obtained from the free vibration analysis for the system with FM are used for the aeroelastic response. The basic idea of this method is that the local deformation due to large mass enables us to afford the structural changes.

Free vibration equation of motion of an n DOF system with FMs is given as

$$[M + M_f]\{\ddot{u}\} + [K]\{u\} = \{0\} \tag{1}$$

The FM M_f is added to the DOF where structural change occurs. The value of FM is large enough not to induce numerical difficulty. Normal mode analysis for Eq. (1) gives a set of n_f low-frequency fictitious vibration mode $[\phi_f]$. Then the generalized mass and stiffness matrix are given as

$$\begin{aligned}[GM_f] &= [\phi_f]^T[M + M_f][\phi_f] \\ [GK_f] &= [\omega_f]^2[GM_f] = [\phi_f]^T[K][\phi_f]\end{aligned} \tag{2}$$

A coordinate transformation is then performed to clean out the FMs and to form an actual basic case whose stiffness matrix may differ from those of the nominal case by $[\Delta K_b]$. The transformation is based on the natural frequencies $[\omega_b]$ and eigenvectors $[\chi_b]$ associated with the equation of free undamped vibration in modal coordinates

$$\begin{aligned}&([GM_f] - [\phi_f]^T[M_f][\phi_f])\{\ddot{\xi}_f\} + ([GK_f] \\ &\quad + [\phi_f]^T[\Delta K_b][\phi_f])\{\xi_f\} = \{0\}\end{aligned} \tag{3}$$

The mode shapes calculated for the FM finite element model are transformed to the basic case by

$$[\phi_b] = [\phi_f][\chi_b] \tag{4}$$

The basic case mode shapes $[\phi_b]$ serve as a constant set of structural generalized coordinates throughout the response analysis.

Transient Aerodynamic Force

The linear relationship between the aerodynamic force acting on the nodal point and the vertical displacement of the nodal point is obtained as follows:

$$\{F\} = q[Q]\{u\} \tag{5}$$

The structural displacement is transformed into modal coordinate as follows:

$$\{u\} = [\phi_b]\{\underline{u}\} \tag{6}$$

Then, the generalized aerodynamic force can be written as

$$[\underline{F}] = [\phi_b]^T[F][\phi_b] = q[\phi_b]^T[Q][\phi_b]\{\underline{u}\} = q[\underline{Q}]\{\underline{u}\} \tag{7}$$

Generally, unsteady aerodynamic influence coefficient matrix is calculated for discrete reduced frequency k rather than calculated as a continuous function of the circular frequency ω. Thus, the aerodynamic influence coefficient matrices should be approximated as a rational function. There are many methods of rational function approximation, but Roger and Abel's method[14] is used here for simplicity and fast computation time. The approximation form is as follows:

$$[\underline{Q}(k)] = [A_1] + [A_2](ik) + [A_3](ik)^2 + \sum_{m=4}^{M+3} \frac{[A_m](ik)}{(ik) + k_m} \tag{8}$$

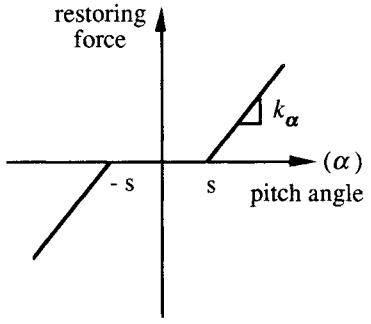

Fig. 1 Freeplay nonlinearity.

Here, A_i are calculated from least-square fit. k_m are constants to be determined for best fit. Simplex direct search method[17] is used to determine k_m for minimizing fitting error.

Transient aerodynamic force of an arbitrary wing motion can be written as follows:

$$\underline{F}(t) = q\left([A_1] + \sum_{m=4}^{M+3}[A_m]\right)\underline{u}(t) + q[A_2]\left(\frac{b}{U_\infty}\right)\dot{\underline{u}}(t) + q[A_3]\left(\frac{b}{U_\infty}\right)^2\ddot{\underline{u}}(t) - q\sum_{m=4}^{M+3}[A_m]p_m\underline{z}_m \tag{9}$$

where

$$p_m = \left(\frac{b}{U_\infty}\right)k_m, \qquad \underline{z}_m = \int_0^t \underline{u}(\tau)e^{-p_m(t-\tau)}\,d\tau$$

$$\begin{Bmatrix} \{\dot{\underline{v}}\} \\ \{\dot{\underline{u}}\} \\ \{\dot{\underline{z}}_4\} \\ \vdots \\ \{\dot{\underline{z}}_{M+3}\} \end{Bmatrix} = \begin{bmatrix} -[\hat{M}]^{-1}[\hat{C}] & -[\hat{M}]^{-1}[\hat{K}] & -[\hat{M}]^{-1}[\hat{A}_4] & \cdots \\ [I] & [0] & [0] & \cdots \\ [0] & [I] & -p_4[I] & [0] \\ \vdots & \vdots & [0] & \ddots \\ [0] & [I] & [0] & \cdots \end{bmatrix}$$

$$\begin{bmatrix} -[\hat{M}]^{-1}[\hat{A}_{M+3}] \\ [0] \\ [0] \\ \vdots \\ -p_{M+3}[I] \end{bmatrix} \begin{Bmatrix} \{\underline{v}\} \\ \{\underline{u}\} \\ \{\underline{z}_4\} \\ \vdots \\ \{\underline{z}_{M+3}\} \end{Bmatrix} - [\hat{M}]^{-1} \begin{Bmatrix} \{\phi_b\}^T\{f(\alpha)\} \\ \{0\} \\ \{0\} \\ \vdots \\ \{0\} \end{Bmatrix} \tag{18}$$

Equation of motion for aeroelastic system with concentrated structural nonlinearity is written as follows:

$$[M]\{\ddot{u}\} + [C]\{\dot{u}\} + \{R(u)\} = \{F\} \tag{10}$$

where $\{R(u)\}$ is elastic restoring force vector that is a function of displacement. For piecewise nonlinearity, restoring force can be written as follows:

$$\{R(u)\} = [K]\{u\} + \{f(\alpha)\} \tag{11}$$

where $[K]$ is a linear stiffness matrix without freeplay, and $\{f(\alpha)\}$ is the restoring force vector whose elements are zero except for nonlinear element. For freeplay nonlinearity shown in Fig. 1, $\{f(\alpha)\}$ is given as follows:

$$\{f(\alpha)\} = \begin{cases} K_\alpha(\alpha - s), & \alpha > s \\ 0, & -s < \alpha < s \\ K_\alpha(\alpha + s), & \alpha < -s \end{cases} \tag{12}$$

The transformation of Eq. (10) into the modal coordinate ($\{u\} = [\phi_b]\{\underline{u}\}$) gives

$$[GM]\{\ddot{\underline{u}}\} + [GC]\{\dot{\underline{u}}\} + \{GR(\underline{u})\} = [\underline{F}] \tag{13}$$

where the generalized mass, damping matrix, and restoring force vector are as follows:

$$[GM] = \{\phi_b\}^T[M]\{\phi_b\}, \qquad [GC] = \{\phi_b\}^T[C]\{\phi_b\}$$
$$[GR(u)\} = [GK]\{u\} + \{\phi_b\}^T\{f(\alpha)\} \tag{14}$$

Let us define the state variable and matrices as follows:

$$\{\underline{v}\} = \{\dot{\underline{u}}\} \tag{15a}$$
$$\{\dot{\underline{v}}\} = \{\ddot{\underline{u}}\} \tag{15b}$$
$$[\hat{M}] = [GM] - q\left(\frac{b}{U_\infty}\right)^2[A_3] \tag{15c}$$
$$[\hat{C}] = [GC] - q\left(\frac{b}{U_\infty}\right)[A_2] \tag{15d}$$
$$[\hat{K}] = [GK] - q[\bar{A}_1] \tag{15e}$$
$$[\hat{A}_m] = qp_m[A_m] \tag{15f}$$
$$[\bar{A}_1] = [A_1] + \sum_{m=4}^{M+3}[A_m] \tag{15g}$$

Rearranging the previous formulas, Eq. (13) can be written as

$$[\hat{M}]\{\dot{\underline{v}}\} = -[\hat{C}]\{\underline{v}\} - [\hat{K}]\{\underline{u}\} - \{\phi_b\}^T\{f(\alpha)\} + \sum_{m=4}^{M+3}[\hat{A}_m]\{\underline{z}_m\} \tag{16}$$

$$\dot{\underline{z}}_m(t) = \underline{u}(t) - p_m\underline{z}_m(t), \qquad \underline{z}_m(0) = 0 \tag{17}$$

Combining Eqs. (16) and (17), we get the final state-space equation as follows:

The number of equations in Eq. (18) is $(2 + M) \times N$ (M = number of simple pole, N = number of normal mode). Integrating Eq. (18) gives the time response for a nonlinear system. Here, the 5–6th-order Runge–Kutta–Verner algorithm is used for the adaptive integration step.

Results and Discussion

As a numerical example, a control fin-type flexible wing is used for nonlinear aeroelastic analysis. The model configuration is given in Fig. 2. The specification of the model is as follows:

Material: aluminum (E = 72.4 GPa, G = 26.2 GPa, ρ = 2713 kg/m^3
16 eight-node isoparametric finite element mesh (4 × 4)
49 doublet lattice aerodynamic mesh (7 × 7)
Mach number M = 0
Nonlinear spring at the root hinge (pitch DOF): k_α = 120 Nm/rad
Root chord thickness = 3 mm
Tip chord thickness = 1.5 mm

Free Vibration Analysis

The results for free vibration analysis are presented in Table 1. Comparison has been made between the results of the direct model and the FM model. The direct model has two types of spring constant. The first model has a torsional spring (k_α = 120 Nm/rad) at the rotational axis. The second type has a zero spring, which has a rigid body mode corresponding to zero natural frequency (the first mode). The results of the direct model with a spring (k_α = 120 Nm/rad) was obtained

Table 1 Natural frequencies of control fin for various computation conditions[a]

Mode	Direct model k_α = 120 Nm/rad	Direct model k_α = 0 Nm/rad	FM model
1	77.0538	0	77.0538
2	131.9821	100.8044	132.1264
3	391.6683	391.0574	391.6763
4	450.1578	434.0840	450.5857
5	700.9876	700.4392	700.9638
6	957.5791	949.0727	2745.346

[a]Unit = Hz.

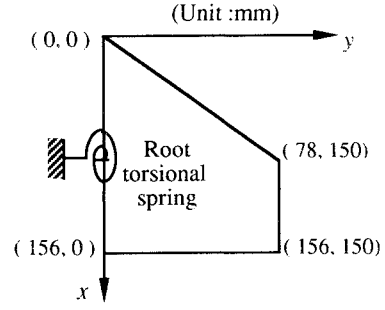

Fig. 2 Model configuration.

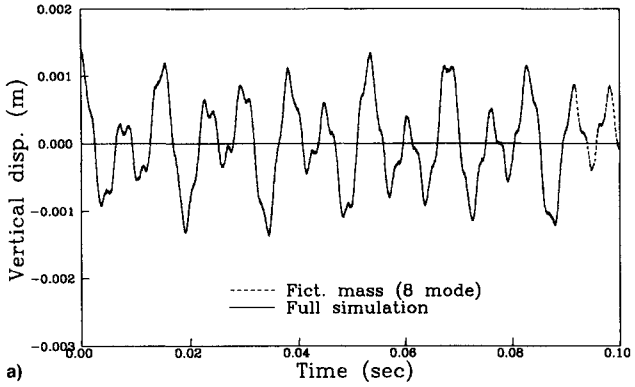

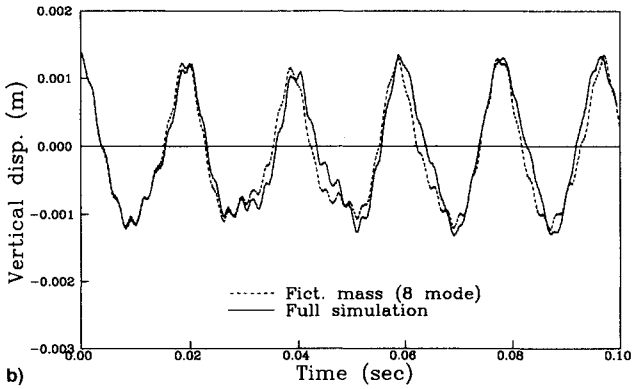

Fig. 3 Time responses of the free oscillation (α_0 = 1 deg): s/α_0 = a) 0.0 and b) 0.5.

by the finite element model without using any FM. The results of an FM model are obtained by using the FM of 50,000 multiple of the corresponding inertia at the rotational axis. Natural frequencies of the FM model are in a good agreement with those of the direct model except the sixth mode. The sixth natural frequency of FM model is large because the large FM model causes local distortion.

The time response of the free oscillation for the system in Fig. 2 is given in Fig. 3. Here, four (2 × 2) eight-node ele-

Table 2 Comparison of flutter speeds between various methods

Method	Flutter speed, m/s	Flutter frequency, Hz	Reduced frequency
V-g	140.5	113.6	0.397
Time (direct)	141.0	114.0	——
Time (FM)	141.0	114.0	——
Time (nominal)	168.0	——	——

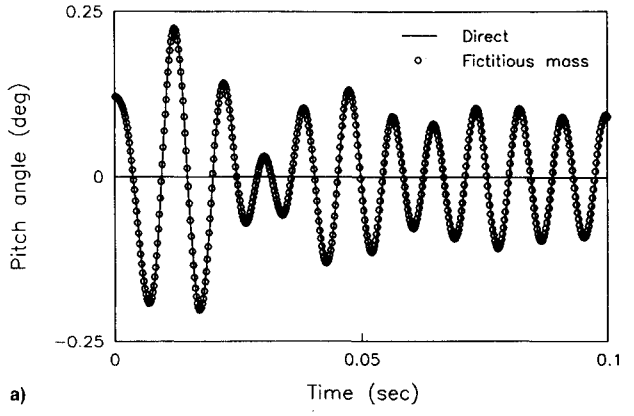

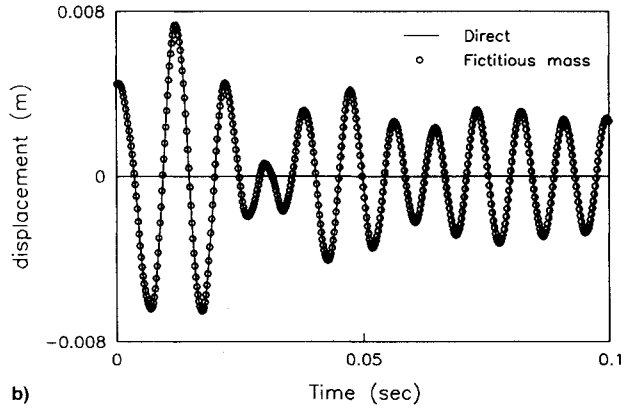

Fig. 4 Time responses of the linear model (U_∞ = 140 m/s, initial condition = 0.001 × the amplitude of the first mode): a) root pitch angle history and b) tip displacement history.

ments were used for time simulation. The initial condition is a rigid pitch rotation of 1 deg. Figure 3a shows the displacements of the root leading edge for the linear system (s/α_0 = 0). In this case, the results of the FM are completely corresponding to those of the full simulation. The full simulation is obtained from the direct model without using the FM. The results of the FM are obtained by using eight modes. Therefore, a tremendous computation time has been saved compared with the full simulation, which has 63 DOF. Figure 3b shows the results for the nonlinear system with the gap/amplitude ratio of 0.5 (s/α_0 = 0.5). The results of the FM are reasonably accurate and the entire wave forms by the FM method are very close to those of the full simulation.

Linear Flutter Analysis

To verify the computational scheme and program, a linear flutter analysis for a system given in Fig. 2 is performed. The spring coefficient at the root of the wing is 120 Nm/rad. From the mode convergency test, it was known that six lowest modes gave accurate results. The results are given in Table 2. V-g in Table 2 means the traditional V-g method. Time (direct) in Table 2 means the time integration method for the direct model. The direct model uses mode shapes of the direct model with linear spring, which gives the correct and accurate results. Time (nominal) is the result obtained by using the modes of

the direct linear model without spring. Time (FM) is the result obtained by using mode shapes of the FM model without spring. In the nominal and the FM model, the spring stiffness is added by modal coupling during the time integration. The results of the FM model are in a good agreement with those of the direct model and the V-g method. The nominal model has a large error compared with other methods. To demonstrate the accuracy of the FM model, a time history of flutter results is shown in Fig. 4. Figure 4a shows the time history of the pitch angle at the wing root and Fig. 4b shows the time history of the displacement at the root leading edge. The results of the FM model are very accurate compared with those of the direct model. Therefore, the FM model gives very accurate results when only six modes are used. Hence, the effect of the local stiffness changes due to nonlinear freeplay can be accurately calculated by the FM method.

Nonlinear Flutter Analysis

The flutter analysis of the nonlinear model with a root pitch freeplay nonlinearity has been investigated. In the nonlinear flutter analysis, the responses are very sensitive to the initial conditions. Thus, the effect of the initial conditions and the freeplay quantity on the aeroelastic response are examined. The computational results for the system of Fig. 2 are given in Figs. 5–10. The initial condition is a rigid pitch angle of 0.1 deg. The pitch angle of the root axis is selected for motion characteristics for convenience. The representative responses for the root pitch angle are dependent on the gap/amplitude ratio, i.e., the freeplay angle to the initial pitch angle. In these figures, the flutter is defined as a divergent oscillation. The chaotic motion means a bounded random-like motion including continual jump behavior. The limit cycle oscillation means a bounded motion consisting of limited number of cycles and amplitudes.

Figure 5 shows the time response of the linear case ($s/\alpha_0 = 0$). When the flow velocity is 135 m/s, the response is damped out as time proceeds. A nearly harmonic oscillation reaches 140 m/s. The divergent oscillation occurs at 145 m/s. The flutter speed can be defined as the speed slightly higher than 140 m/s. The overall feature of the response is monotonous in this linear case.

Figure 6 represents the time response of the nonlinear case ($s/\alpha_0 = 0.05$). In this case, the limit cycle oscillation is the dominant feature. A typical limit cycle oscillation occurs at 130 m/s. The describing function technique can be applied in this region. The response approaches to a limit cycle oscillation at the speed of 135 m/s. Near the speed of 140 m/s, the motion diverges.

Figure 7 illustrates the time response of the nonlinear case of the gap/amplitude ratio ($s/\alpha_0 = 0.2$). In this gap/amplitude ratio, the chaotic behavior is observed instead of the limit cycle oscillation. In this case the equivalent stiffness approach based on the describing function cannot be applied. At the speed of 140 and 145 m/s, the motion is limited inside of the

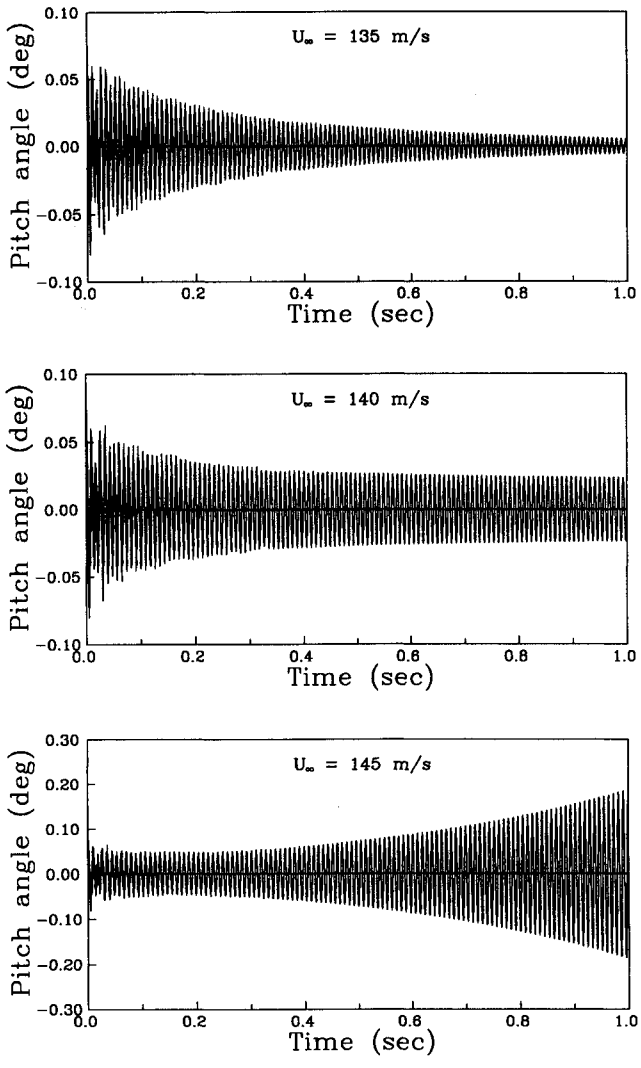

Fig. 5 Time responses of the linear model for various velocities ($s/\alpha_0 = 0$).

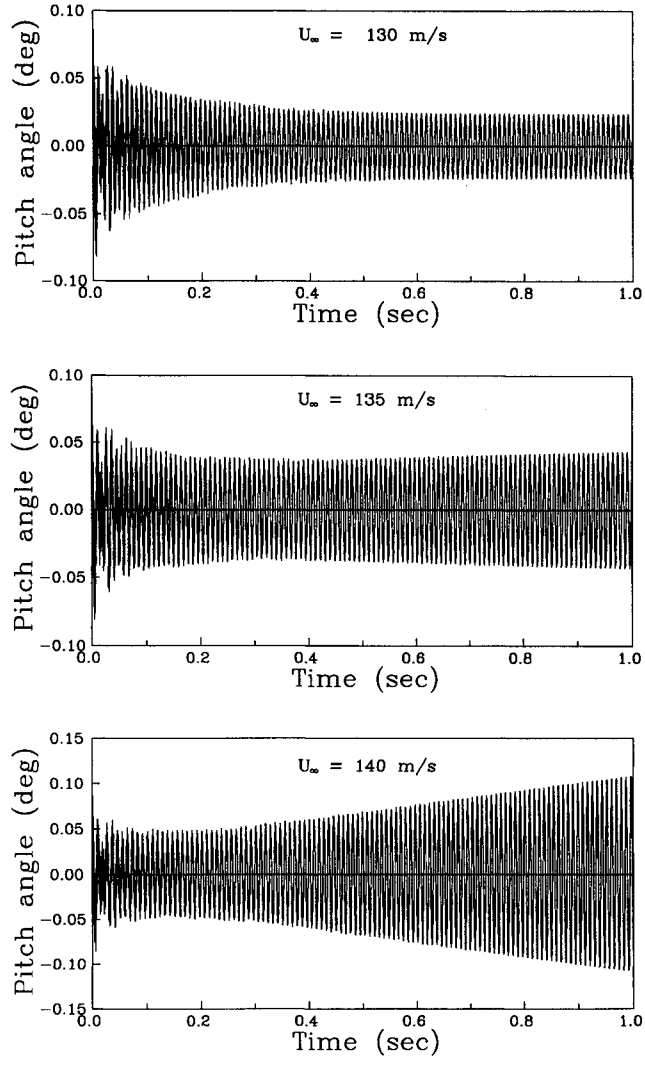

Fig. 6 Time responses of the nonlinear model for various velocities ($s/\alpha_0 = 0.05$).

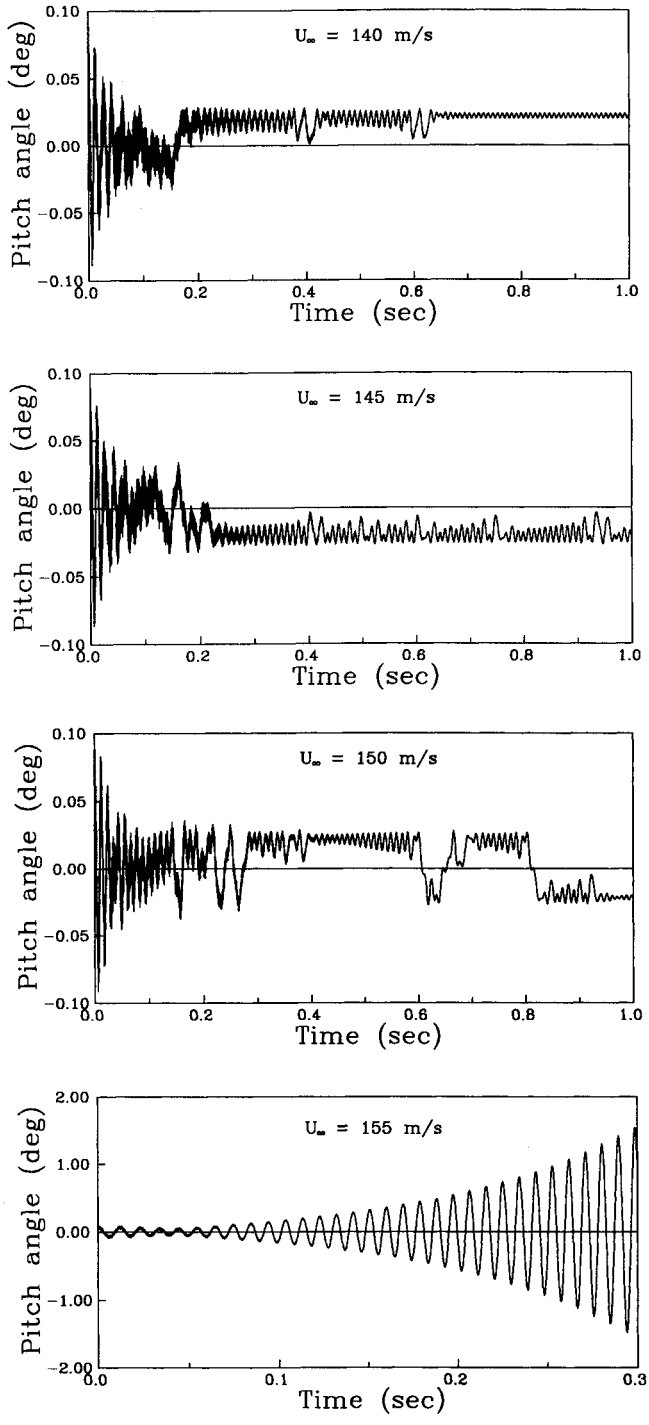

Fig. 7 Time responses of the nonlinear model for various velocities (s/α_0 = 0.2).

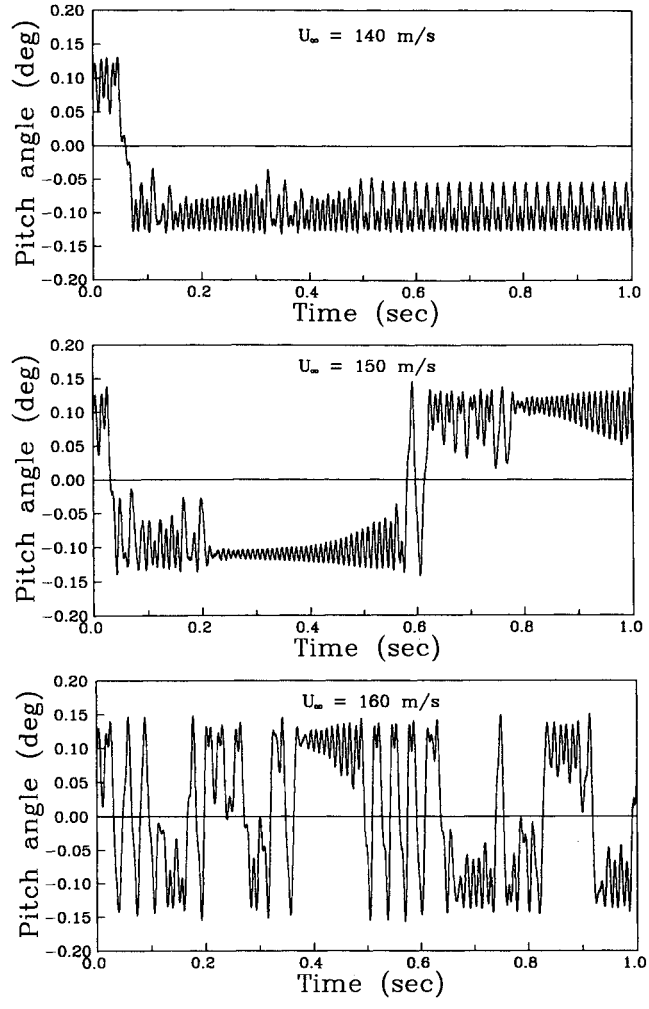

Fig. 8 Time responses of the nonlinear model for various velocities (s/α_0 = 1.0).

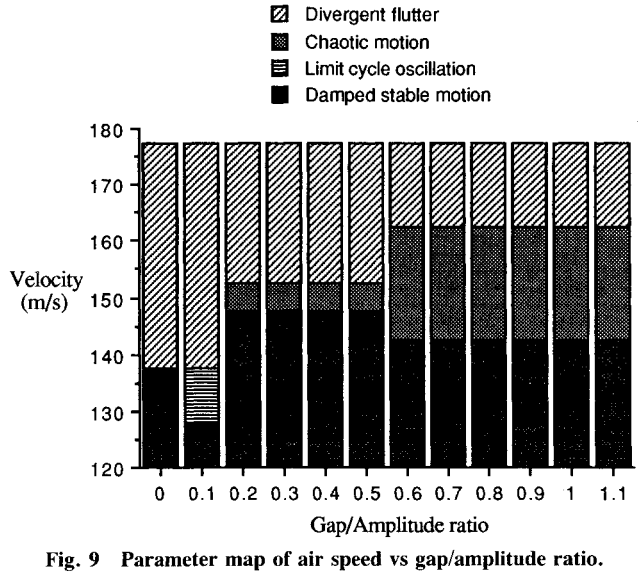

Fig. 9 Parameter map of air speed vs gap/amplitude ratio.

freeplay angle. Here, the freeplay angle is ±0.02 deg. The jump phenomenon is observed at 150 m/s. In this study, a continual jump motion is classified as the chaotic motion. The presence of chaotic motion around the two corners of freeplay nonlinearity is observed. The abrupt divergent motion occurs at 155 m/s.

Figure 8 shows the time response of the nonlinear case of the gap/amplitude ratio (s/α_0 = 1.0). In this case, the freeplay angle is the same as the initial pitch angle. As the flow speed increases, the jump phenomenon occurs more frequently. The motions are bounded by the freeplay nonlinearity. The chaotic response is observed for broad velocity band.

Figure 9 describes a parameter map for velocity vs gap/amplitude ratio. All results were obtained when the motion is considered to be settled down. Sustained small oscillations are classified as damped stable motion. For high gap/amplitude ratios (small initial exitation), a wide range of chaotic behavior is observed. Divergent flutter occurs abruptly after the chaotic motion. When the gap/amplitude ratio becomes higher than 0.6, the motion characteristics are alike. Limit cycle oscillation is observed at the low gap/amplitude ratio (s/α_0 = 0.1).

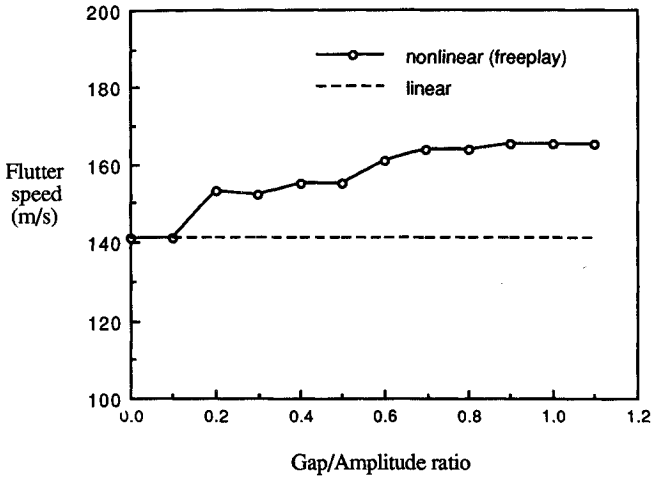

Fig. 10 Divergent flutter speeds of the linear and nonlinear model.

Figure 10 shows the divergent flutter speeds for various gap/amplitude ratios. When the gap/amplitude ratio becomes small, the flutter speed approaches that of the linear case. As the gap/amplitude ratio increases, the flutter speed becomes much higher than that of the linear case.

These results are obtained for a fixed initial angle of attack and variable freeplay quantity. The variable parameter could be an angle of attack with a fixed pitch freeplay quantity. However, these results could be obtained by reinterpreting Figs. 5–10.

Conclusions

The present study dealt with the time domain aeroelastic analysis for a control surface with concentrated structural nonlinearity. The method used in this study can be applied to the arbitrarily shaped wing with multiple nonlinearities. A typical flexible control surface with a single root pitch freeplay is selected for numerical simulation. The free vibration analysis and the linear flutter analysis results show the validity of this method. The FM method is well applied to the system with concentrated nonlinearity and gives accurate results. This method can save a tremendous amount of computation time when a few number of modes are used for the nonlinear flutter analysis.

Nonlinear flutter analysis shows that the responses are very sensitive to the amount of the freeplay quantity. The limit cycle oscillations are observed at low gap/amplitude ratios. The chaotic motions are observed for large gap/amplitude ratios. As the gap/amplitude ratio increases, the flutter speed of the nonlinear system becomes higher than that of the linear case.

References

[1]Laurenson, R. M., and Trn, R. M., "Flutter Analysis of Missile Control Surfaces Containing Structural Nonlinearities," *AIAA Journal*, Vol. 18, No. 10, 1980, pp. 1245–1251.

[2]Hauenstein, A. J., Laurenson, R. M., and Gubser, J. L., "Investigations of an Asymptotic Expansion Technique to Analyze Surfaces with Structural Nonlinearities," Final Rept. Air Force Office of Scientific Research (AFSOR) Contract F49620-84-C-0123.

[3]Woolston, D. S., Runyan, H. W., and Andrews, R. E., "Some Effects of System Nonlinearities in the Problem of Aircraft Flutter," NACA TN 3539, Oct. 1957.

[4]McIntosh, S. C., Reed, R. E., Jr., and Rodden, W. P., "Experimental and Theoretical Study of Nonlinear Flutter," *Journal of Aircraft*, Vol. 18, No. 12, 1981, pp. 1057–1063.

[5]Lee, C. L., "An Iterative Procedure for Nonlinear Flutter Analysis," *AIAA Journal*, Vol. 24, No. 5, 1986, pp. 833–840.

[6]Zhao, L. C., and Yang, Z. C., "Analysis of Limit Cycle Flutter of an Airfoil in Incompressible Flow," *Journal of Sound and Vibration*, Vol. 123, No. 1, 1990, pp. 1–13.

[7]Zhao, L. C., and Yang, Z. C., "Chaotic Motions of an Airfoil with Non-Linear Stiffness in Incompressible Flow," *Journal of Sound and Vibration*, Vol. 138, No. 2, 1990, pp. 245–254.

[8]Brase, L. O., and Eversman, W., "Application of Transient Aerodynamics to the Structural Nonlinear Flutter Problem," *Journal of Aircraft*, Vol. 25, No. 11, 1988, pp. 1060–1068.

[9]Hauenstein, A. J., Laurenson, R. M., Eversman, W., Galecki, G., Qumei, I., and Amos, A. K., "Chaotic Response of Aerosurfaces with Structural Nonlinearities," *Proceedings of the AIAA/ASME/ASCE/AHS/ASC 31st Structures, Structural Dynamics, and Materials Conference*, AIAA, Washington, DC, 1990, pp. 1530–1539 (AIAA Paper 90-1034).

[10]Hauenstein, A. J., Zara, J. A., Eversman, W., and Qumei, I., "Chaotic and Nonlinear Dynamic Response of Aerosurfaces with Structural Nonlinearities," *Proceedings of the AIAA/ASME/ASCE/AHS/ASC 33rd Structures, Structural Dynamics, and Materials Conference*, AIAA, Washington, DC, 1992, pp. 2367–2375 (AIAA Paper 92-2547).

[11]Price, S. J., Lee, B. H. K., and Alighanbari, H., "An Analysis of the Post-Instability Behaviour of a Two-Dimensional Airfoil with a Structural Nonlinearity," *Proceedings of the AIAA/ASME/ASCE/AHS/ASC 34th Structures, Structural Dynamics, and Materials Conference*, AIAA, Washington, DC, 1993, pp. 1452–1460 (AIAA Paper 93-1474).

[12]Price, S. J., Lee, B. H. K., and Alighanbari, H., "The Aeroelastic Response of a Two-Dimensional Airfoil with Bilinear and Cubic Structural Nonlinearities," *Proceedings of the AIAA/ASME/ASCE/AHS/ASC 35th Structures, Structural Dynamics, and Materials Conference*, AIAA, Washington, DC, 1994, pp. 1771–1780 (AIAA Paper 94-1546).

[13]Albano, E., and Rodden, W. P., "A Doublet-Lattice Method for Calculating Lifting Disturbances in Subsonic Flow," *AIAA Journal*, Vol. 2, No. 2, 1969, pp. 279–285.

[14]Abel, I., "An Analytical Technique for Predicting the Characteristics of a Flexible Wing Equipped with an Active Flutter Suppression System and Comparison with Wind Tunnel Data," NASA TP 1367, Feb. 1979.

[15]Karpel, M., and Wieseman, C. D., "Modal Coordinates for Aeroelastic Analysis with Large Local Structural Variations," *Journal of Aircraft*, Vol. 31, No. 2, 1994, pp. 396–403.

[16]Karpel, M., and Wieseman, C. D., "Time Simulation of Flutter with Large Stiffness Changes," *Journal of Aircraft*, Vol. 31, No. 2, pp. 404–410.

[17]Nelder, J. A., and Mead, R., "A Simplex Method for Function Minimization," *The Computer Journal*, Vol. 7, No. 2, 1969, pp. 279–285.